Pergamon

Geochimica et Cosmochimica Acta, Vol. 65, No. 9, pp. 1367–1379, 2001

0016-7037/01 $20.00 + .00

PII S0016-7037(00)00623-2

Kinetics of reductive bulk dissolution of lepidocrocite, ferrihydrite, and goethite

OLE LARSEN*,† and DIEKE POSTMA

Department of Geology and Geotechnical Engineering, Groundwater Research Centre, Technical University of Denmark, Building 204, DK-2800 Kgs Lyngby, Denmark

(*Received June* 21, 2000; *accepted in revised form October* 27, 2000)

Abstract—The variation in Fe-oxide reactivity was investigated by studying the kinetics of bulk reductive dissolution of a suite of synthetic Fe-oxides in 10 mM ascorbic acid at pH 3. The Fe-oxides comprised three different ferrihydrites, five lepidocrocites, and a poorly crystalline goethite. During one of the reduction experiments, lepidocrocite crystals were subsampled and the change in crystal habit and size distribution was studied by transmission electron microscopy.

The rate of complete dissolution was described by the function $J/m_0 = k'(m/m_0)^{\gamma}$ where J is the overall rate of dissolution (mol/s), m_0 the initial amount of iron oxides, and m/m_0 the undissolved mineral fraction. Rate laws were derived for the different iron oxides and showed a variation in initial rates of about two orders of magnitudes; 2-line ferrihydrites being most reactive with $k' = 7.6–6.6 \times 10^{-4} \cdot s^{-1}$, whereas the initial rate for 6-line ferrihydrite is an order of magnitude lower $7.4 \times 10^{-5} \cdot s^{-1}$ and comparable to the quite homogeneous group of lepidocrocites ($3.2–8.1 \times 10^{-5} \cdot s^{-1}$) with finally the initial rate of goethite being one order of magnitude lower again ($5.4 \times 10^{-6} \cdot s^{-1}$). The transmission electron microscopy results for lepidocrocite showed strong etch-pitting of the crystals parallel to the c-axis resulting ultimately in disintegration of the crystals.

For the different iron oxides, the initial rate was independent of the specific surface area, emphasizing the importance of the crystal structure for the dissolution rate. However, among the lepidocrocites the initial rate was proportional to the specific surface area.

The exponent, γ was found to vary from a value near 1.0 for one of the 2-line ferrihydrites, two of the lepidocrocites and the goethite, to values close to 2.3 for the other 2-line ferrihydrite and the 6-line ferrihydrite. Thus, the largest variation in reduction rate during bulk dissolution is found for ferrihydrite. For the lepidocrocites, the preparations that predominantly consist of single domain crystals yielded γ-values near 1.4–1.6, whereas the multidomainic crystal preparations yielded values of 1.0–1.1. The parameter γ collects the effects of factors, such as the crystal geometry, the particle size distribution and the reactive site density. The relative importance of these factors was evaluated and particularly the particle size distribution appears to be of importance for iron oxides.

1. INTRODUCTION

Iron oxide is an important terminal electron acceptor for the oxidation of organic matter in both aquifers (Lyngkilde and Christensen, 1992; Jakobsen and Postma, 1999), soils (van Breemen, 1988), and marine sediments (Canfield et al., 1993). Factors that control the reduction rate of iron oxides in a sediment are many and they comprise the reactivity of organic matter and availability of reductants. Often the reduction of iron oxides is mediated by microorganisms (Munch and Ottow, 1980; Albrechtsen and Christensen, 1994; Lovley, 1991; Roden and Zachara, 1996; Roden and Urrutia, 1999). In addition, the pool of iron oxide present in sediments is heterogeneous and the reactivity of iron oxides influences to what extent they are reduced (Canfield et al., 1992; Postma, 1993; Deng and Stumm, 1994; Postma and Jakobsen, 1996; Raiswell and Canfield, 1998).

The mechanisms for reductive dissolution of iron oxides have been studied in detail for different reductants, complexing agents, and iron oxides, and a wide variation in observed rates has been reported (Banwart et al., 1989; Sulzberger et al., 1989; Dos Santos Afonso et al., 1990; Suter et al., 1991; Biber et al., 1994; Yao and Millero, 1996; Nowack and Sigg, 1997). Typically, these studies have been carried out as initial rate experiments, i.e., the percentage of mineral dissolved in the course of the experiment is negligible and the surface properties of the Fe-oxide mineral are considered as a constant. This is a major simplification compared to what happens in a natural environment, where often a significant part of the iron oxide present is reduced. For example, in the upper layers of a marine sediment high in reactive organic matter, nearly all iron oxide present becomes reduced within the upper metre (Canfield, 1989). Also in aquifers, a organic pollutant plume may quantitatively reduce the Fe-oxides from the aquifer sediment as it migrates downstream (Heron et al., 1994). When a significant part of the iron oxides present in the sediment is reduced, selective dissolution of the most reactive material will occur and changes in both the mineralogy and the particle size distribution of the remaining pool of iron oxide are the result. Due to the removal of the most reactive material, the rate of iron oxide reduction will decrease. Therefore the bulk reductive dissolution kinetics of iron oxides are of importance to understand the cycling of iron oxides in sediments (Postma, 1993; Cornell and Schwertmann, 1996).

The effects of both the reductant and the crystal properties on

* Author to whom correspondence should be addressed: (olarsen@mpi-bremen.de).
† *Present address:* Max Planck Institute for Marine Microbiology, Celsiusstr. 1, D-28359 Bremen, Germany.

the overall reaction rate are collected in the general rate law for mineral dissolution by Christoffersen and Christoffersen (1976):

$$J = \frac{-dm}{dt} = km_0 f\left(\frac{m}{m_0}\right) g(C) \quad (1)$$

Here J is the overall rate of dissolution (mol/s); m, the amount of undissolved crystals (mol); t, time (s); k, the rate constant (s^{-1}), and m_0 the initial mass of crystals (mol). $f(m/m_0)$ is a function of the remaining fraction of mineral mass and $g(C)$ is a function of the solution composition. An important feature of Eqn. 1 is that the effects of the crystals and of the solution composition on the rate are separated into different terms. Accordingly, during an initial rate experiment, $m/m_0 = 1$ and $f(m/m_0)$ becomes a constant. Therefore, the effect of solution composition on the overall rate can be studied separately from effects due to crystal changes during dissolution.

$f(m/m_0)$ is a function of changing crystal sizes, morphology, reactive site density, etc. Only for populations of monodisperse crystals of isometric shape, such as spheres or cubes, that dissolve homogeneous over their entire surface area does $f(m/m_0)$ take a simple form. As the crystals dissolve, the surface area decreases and the relation between surface area and mass predicts $f(m/m_0)$ to be $(m/m_0)^{2/3}$. In its integrated form, this is equal to the cubic rate law that has been used to fit bulk dissolution data for iron oxides (e.g., Cornell et al., 1975; Cornell et al., 1976; Sidhu et al., 1989). Not surprisingly the cubic rate law is rarely able to match more than part of the dissolution data. A number of rate laws that relate various surface processes such as diffusion and surface nucleation to specific rate laws are available (Cornell and Schwertmann, 1996), but due to the complexity of the problem these rate laws are rarely useful. Instead $f(m/m_0)$ is mostly used in a more empirical sense and is then often expressed by the exponential function $(m/m_0)^{\gamma}$. For example Christoffersen and Christoffersen (1976) found that $\gamma = 1.16$ for gypsum dissolution, Christoffersen et al. (1978) $\gamma = 0.6$ for hydroxyapatite dissolution and Postma (1993) $\gamma = 1.1$ for ferrihydrite reduction by ascorbic acid.

At a high ascorbic acid concentration (>5 mM) the surface of the iron oxide gets saturated with ascorbic acid and the reduction rate becomes then independent of the ascorbic acid concentration (Banwart et al., 1989; Postma, 1993). In that case $g(C)$ is a constant and the effect of crystal reactivity ($(m/m_0)^{\gamma}$) on the rate can be studied separately. The use of ascorbic acid as reductant does in that case not affect the dissolution rate in any other way than contributing to the absolute value of the rate constant k. By using this approach, the dissolution kinetics of some common iron oxides has been investigated during complete reductive dissolution in excess (10 mM) ascorbic acid. The minerals used comprise three different ferrihydrites, five different lepidocrocites and a poorly crystalline goethite. In addition, the factors that influence the change in the rate during complete dissolution of a polydisperse crystal population are evaluated. The overall purpose of this study is to explore the importance of bulk dissolution kinetics of iron oxides. In combination, information on how $g(C)$ and $f(m/m_0)$ respectively affect the reduction rate of iron oxides may improve our understanding of iron cycling in natural sediments.

Table 1. Selected synthesis parameters for five different lepidocrocites (L-1–L-5).

	Temp °C	Cl/Fe	pH
L-1	25	2	6.0
L-2	10	2	6.0
L-3	15	6	5.5
L-4	20	8	5.5
L-5	20	8	5.5

2. METHODS

2.1. Synthesis of Iron Oxides

Two preparations of 2-line ferrihydrite were synthesized from 0.1 M $FeCl_3$, following Schwertmann and Cornell (1991). A 6-line ferrihydrite was synthesized by plunging a 75°C $FeCl_3$ (0.03 M) solution into cold water (0°C), resulting in the slow hydrolysis of iron (Cornell and Schwertmann, 1996).

Five lepidocrocites varying in physical properties were synthesized by oxidizing 0.06 M aqueous Fe^{2+} solutions with pure O_2 (Cornell and Schwertmann, 1996). Differences in crystallinity were induced by varying the temperature, the Fe/Cl ratio and the pH during synthesis (Table 1). The Cl/Fe ratio was varied by adding NaCl to L3–L5 and the pH kept constant by adding 1 M NaOH with an autotitrator (TIM 900 from Radiometer, Copenhagen, Denmark). Sample L-5 was synthesized in two steps, after 90% of the Fe^{2+} was oxidized a second amount of Fe^{2+}, 75% of the initial amount, was slowly added by using a peristaltic pump. Poorly crystalline goethite was synthesized by oxidizing (with air) Fe^{2+} (0.05 M $FeCl_2$) in a 1 M $NaHCO_3$ buffer solution at pH 7.0 (Schwertmann and Cornell, 1991). All the preparations were carried out in plastic laboratory ware to minimize contamination with SiO_2. After their synthesis the iron oxides were washed free of solutes by dialysis. The dialysis bags were made of generated cellulose having a molecular weight cutoff of 12–14000 and supplied by Serva Electrophoresis (Heidelberg, Germany). To avoid contamination, the bags were washed before use by boiling them 20 min in deionized water. The bags were stored in basins continuously flushed with H_2O until the electrical conductivity of the inner solution was lower than 10^{-7} S/m (~2 weeks). The suspensions were stored in the dark at 5°C.

2.2. Characterization of Iron Oxides

The mineral preparations were characterized by using powder X-ray diffraction (XRD), N_2-adsorption, scanning electron microscopy (SEM), and transmission electron microscopy (TEM). Also Fourier transform infrared spectroscopy (FT-IR) and Mössbauer spectroscopy were used for characterization of the iron oxides (Larsen, 1998). The results are not presented here, but are available from the first author upon request.

XRD was performed by using CoKα-radiation on either a Siemens D5000 (Iselin, NJ, USA) or a Philips 1050 diffractometer (Eindhoven, The Netherlands). XRD peak broadening of the lepidocrocite 020 line was used to calculate crystallite size distributions by using the Warren–Averbach method in Win-Crysize (1996). Size and strain can be separated if a diffraction plane is found in differing orders, which is not the case for lepidocrocite. But by assuming that strain effects are negligible, the crystallite size distribution was calculated. A highly crystalline lepidocrocite from Easton, Pennsylvania was used to determine the instrumental line broadening. The specific surface area was estimated by the BET (Brunaur, Emmet and Teller) method, measuring full adsorption and desorption isotherms of pure N_2 in a He carrier on ~0.2 g of sample dried at 50°C under dry gas using a Micromeritics Gemini instrument (Norcross, GA, USA).

SEM was carried out on a Philips XL20 microscope, using specimens sedimented on stubs and coated with platinum. TEM was per-

Table 2. Specific surface area, measured as multipoint BET, for different iron oxides.

Sample	BET m^2/g	k' s^{-1}	γ	F $mol/m^2/s$
2Fer-1	230	7.6×10^{-4}	2.3	4.1×10^{-8}
2Fer-2	250	6.6×10^{-4}	1.0	3.3×10^{-8}
6Fer	205	7.4×10^{-5}	2.5	4.5×10^{-9}
Goethite	153	5.4×10^{-6}	1.0	4.0×10^{-10}
L-1	63	3.9×10^{-5}	1.6	7.0×10^{-9}
L-2	146	8.1×10^{-5}	1.4	6.1×10^{-9}
L-3	112	7.3×10^{-5}	1.4	7.4×10^{-9}
L-4	78	3.2×10^{-5}	1.0	4.6×10^{-9}
L-5	80	4.2×10^{-5}	1.1	5.9×10^{-9}

Parameters of rate laws for iron oxides, obtained by data fits of Eqn. 6 or 7. k' is the rate constant and γ the exponent, and F the initial surface flux or the rate constant normalized to the surface area. 2Fer and 6Fer are respectively 2-line and 6-line ferrihydrites and L-1–L-5, the five different lepidocrocites.

formed by using a Philips EM 300 instrument on suspensions sedimented on carbon coated copper grids. The total amount of iron in the suspensions was determined in a dithionite-citrate-bicarbonate extract (Mehra and Jackson, 1960) by AAS after filtration.

2.3. Experimental Setup

Experiments were carried out in 1.3-L Quickfit™ glass reaction vessels (from Bibby Sterilin) immersed in a thermostated bath (25°C) with a propeller fitted through the top of the vessel. The stirring rate was kept constant for all the experiments. Purified and water-saturated N_2 was continuously passed through the vessel to maintain anoxic conditions. Each experiment was started by filling the reaction vessel with 1.1 L of a anoxic 10 mM ascorbic acid solution, adjusted to pH = 3.000 ± 0.005, followed by addition of stock suspensions of the iron oxides. The reaction of ascorbic acid with iron oxides can be followed by measuring the concentration of released Fe^{2+}, which in acid solution is unlikely to form any precipitate. The samples were in-line filtered through a 0.2-μm membrane filter (cellulose acetate filters from Nalgene) and injected directly into glass vials containing ferrozine. A Na-acetate buffer solution was added to the vials and subsequently Fe^{2+} was determined spectrophotometrically (Stookey, 1970). Preliminary experiments performed in the dark demonstrated that light had no influence on the results.

3. RESULTS

3.1. Synthesized Iron Oxides

Particles of ferrihydrite are very small and due to strong aggregation it is almost impossible to identify single crystals in TEM. The specific surface area of the ferrihydrites (Table 2) was measured to be between 200 and 250 m^2/g by BET corresponding to spherical particles with diameters of 10 to 15 nm. However, due to the hydrous nature of ferrihydrite, the BET method may underestimate the specific surface area of ferrihydrite (Cornell and Schwertmann, 1996). Based on X-ray diffraction, Drits et al. (1993) developed a structural model of ferrihydrite that was confirmed by spectroscopical evidence (EXAFS). The components in this model are composed of crystals with sizes in the nanometre range in agreement with the high surface area of ferrihydrite.

The crystal habit of the lepidocrocite is in all preparations elongated varying from rod-shaped in L-1 to needle-shaped in L-3. Only in preparation L-3 are there in addition hexagons present, a morphology that possibly is inherited from an intermediate green rust precursor of lepidocrocite during synthesis. The sample L-1 clearly contained the largest crystals (200 × 40 nm) and shows the sharpest lines in XRD. In contrast, sample L-2 has the smallest crystals (30 × 10 nm) and the broadest XRD peaks. TEM reveals that lepidocrocite crystals consist of crystallite domains extending along the c-axis and stacked along the a- and b-axis. The samples L-1 to L-3 predominantly contain crystals of single domain nature (~60%) while L-4 and L-5 are multidomainic. The specific surface area of the lepidocrocites ranged between 63 and 146 m^2/g. The sample with the largest crystals L-1 (Fig. 1) also has the lowest specific surface area, whereas L-2 containing the smallest crystals has the highest specific surface area.

The largest single crystals of goethite (100 × 20 nm) showed the typical acicular habit but most of the preparation (>80%) consisted of crystals (50 × 10 nm) organized in dense aggregates without a distinct crystal habit. The surface area of the poorly crystalline goethite was measured as 153 m^2/g, which is in the high end of the range of 8 to 200 m^2/g reported for goethite by Cornell and Schwertmann (1996). The very fine-grained crystals are difficult to describe and measure with TEM so surface areas estimated from the mean crystal size are significantly lower than those measured by the BET method.

The purity of the different mineral preparations was confirmed by XRD as well as Mössbauer spectroscopy and FT-IR (Larsen, 1998).

3.2. Reductive Dissolution Kinetics

Banwart et al. (1989) investigated the reduction of hematite by ascorbic acid at variable concentration and found the reduction rate to depend on the ascorbic acid concentration at the hematite surface. At a high ascorbic acid concentration in the bulk solution, the hematite surface will always be saturated with ascorbic acid and the reductive dissolution rate becomes then independent of the ascorbic acid concentration and is instead controlled by the reactivity of the iron oxide. A similar result was reported for ferrihydrite by Postma (1993). Accordingly the reactivity of different iron oxides can be investigated, and compared, by using a high ascorbic acid concentration. At an ascorbic acid concentration of 10 mM, the reductive dissolution rate of various iron oxides was not influenced by small variations in the ascorbic acid concentration that may occur during the run.

Results of reductive dissolution experiments with ferrihy-

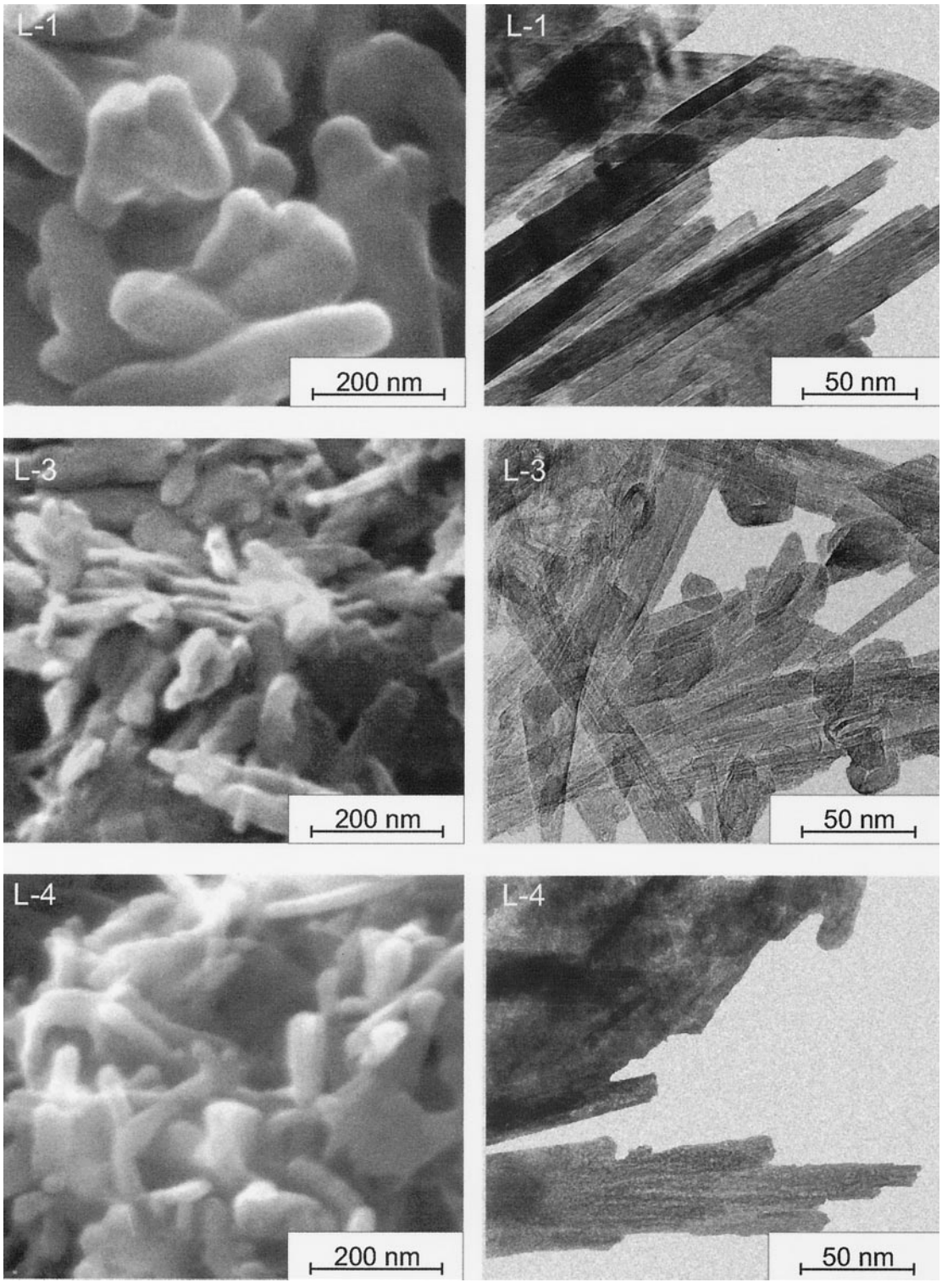

Fig. 1. The morphology of synthetic iron oxides; (a) Scanning electron micrographs of selected lepidocrocites and (b) Transmission electron micrographs (first row, L-1, second row L-3, third row L-4).

drite and 10 mM ascorbic acid at pH 3.000 are presented in Figure 2 and for the different lepidocrocites (L-1 to L-5) and the goethite (G) in Figure 3. The mass of crystals present, m, is displayed normalized to the initial mass, m_0. As shown in Figures 2 and 3, the use of a different m_0 gave in all cases identical curves for m/m_0 vs. time. The rate is accordingly first order with respect to m_0, as was previously shown by Yao and Millero (1996) and Postma (1993). In order to test the impor-

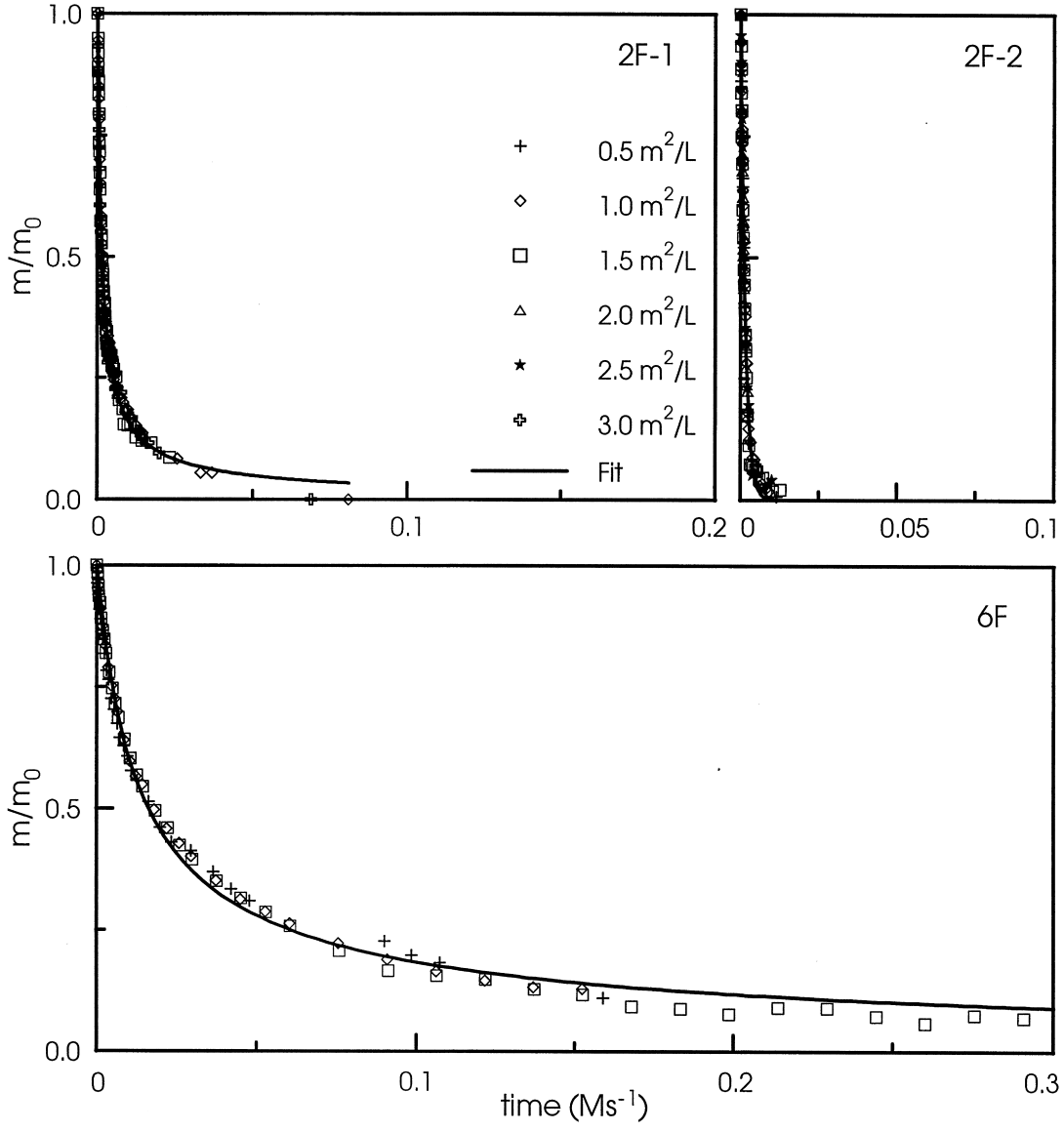

Fig. 2. Reduction of ferrihydrites by 10 mM ascorbic acid at pH 3. m/m_0 is the fraction of undissolved ferrihydrite and M/s is the time in Megaseconds. The lines represent the fit of Eqns. 6 and 7 to the data.

tance of proton-induced dissolution, duplicate experiments were carried out by using 0.001 M HCl instead of the ascorbic acid solution with pH 3. However, HCl always dissolved less than 1% of the iron oxide and reductive dissolution must, therefore, be the predominant pathway in the presence of ascorbic acid.

Among the ferrihydrites (Fig. 2), the 2-line ferrihydrites react much faster than the 6-line ferrihydrite. The 2-line ferrihydrites were synthesized by an apparently identical procedure, but still the preparation 2F-2 reacts faster than 2F-1, the main difference originates from the dissolution of the less reactive fraction. This variability in reactivity is important since in microbiology, experiments often are amended with synthetic ferrihydrite without further characterization (Lovley, 1991; Albrechtsen and Christensen, 1994; Pulgarin and Kiwi, 1995; Thamdrup et al., 1993). The dissolution pattern of the 6-line ferrihydrite 6F is more gradual and at the end of the experiments after 4.5 d, about 5% remained undissolved.

The five lepidocrocites (Fig. 3) display a similar dissolution pattern consisting of an initial stage where the highly reactive fraction is dissolved quickly, followed by a tail representing the dissolution of less reactive material. Samples L-2 and L-3 clearly consist of the most reactive material, whereas sample L-1, that contained the largest crystals, is the slowest one to react. Finally, the poorly crystalline goethite (Fig. 3) reacts much slower than the other iron oxides and at the end of the experiments about 10% of the sample remained undissolved.

3.3. Changing Lepidocrocite Crystals During Dissolution

In order to elucidate the changes in crystal shape and the crystal size distribution during dissolution, subsamples of the

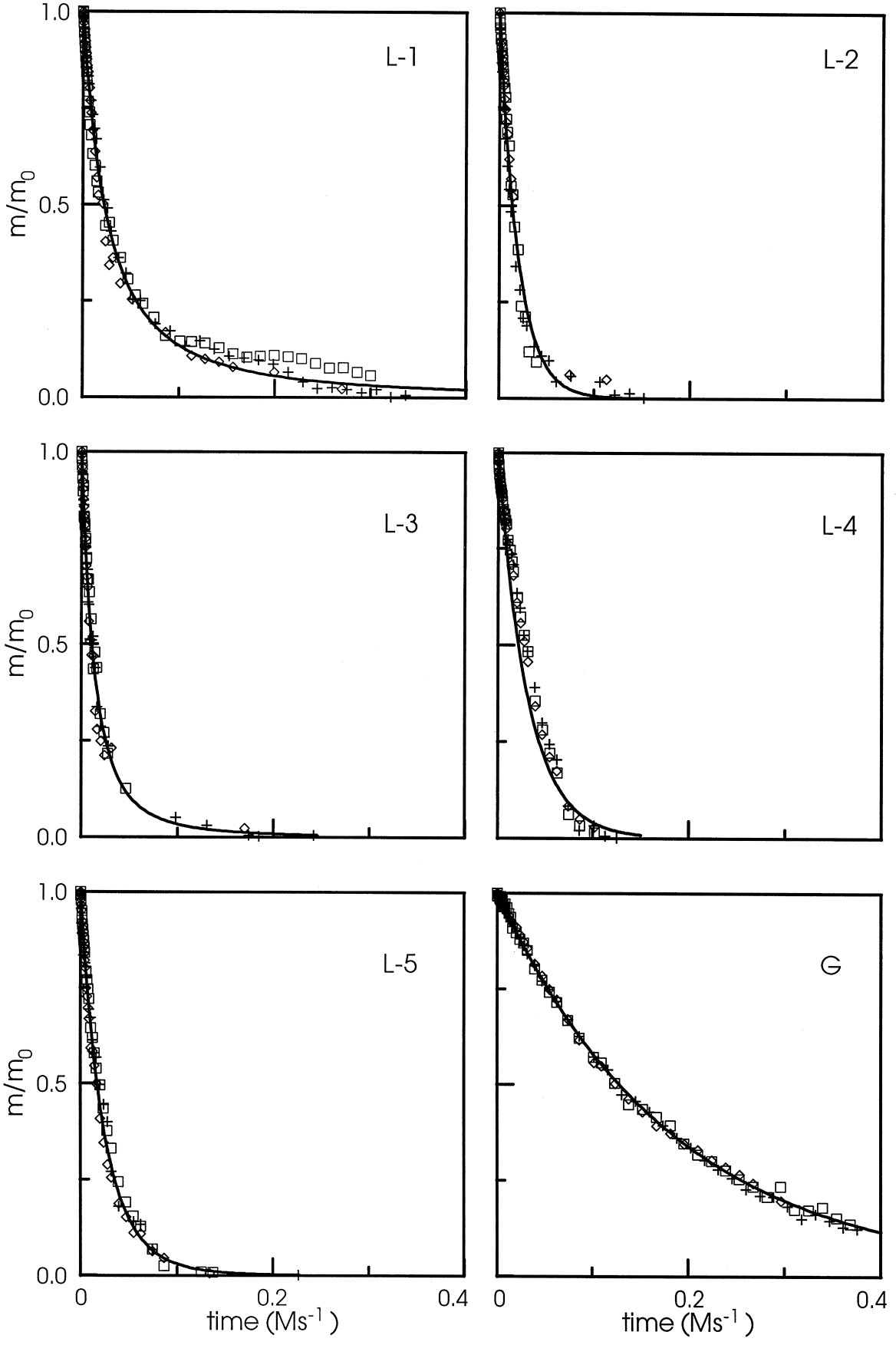

Fig. 3. Reduction of lepidocrocites and goethite by 10 mM ascorbic acid at pH 3. m/m_0 is the fraction of undissolved mineral and M/s is the time in Megaseconds. The lines represent the fit of Eqns. 6 and 7 to the data. Symbols in all graphs correspond to surface area concentration as defined in Fig. 2.

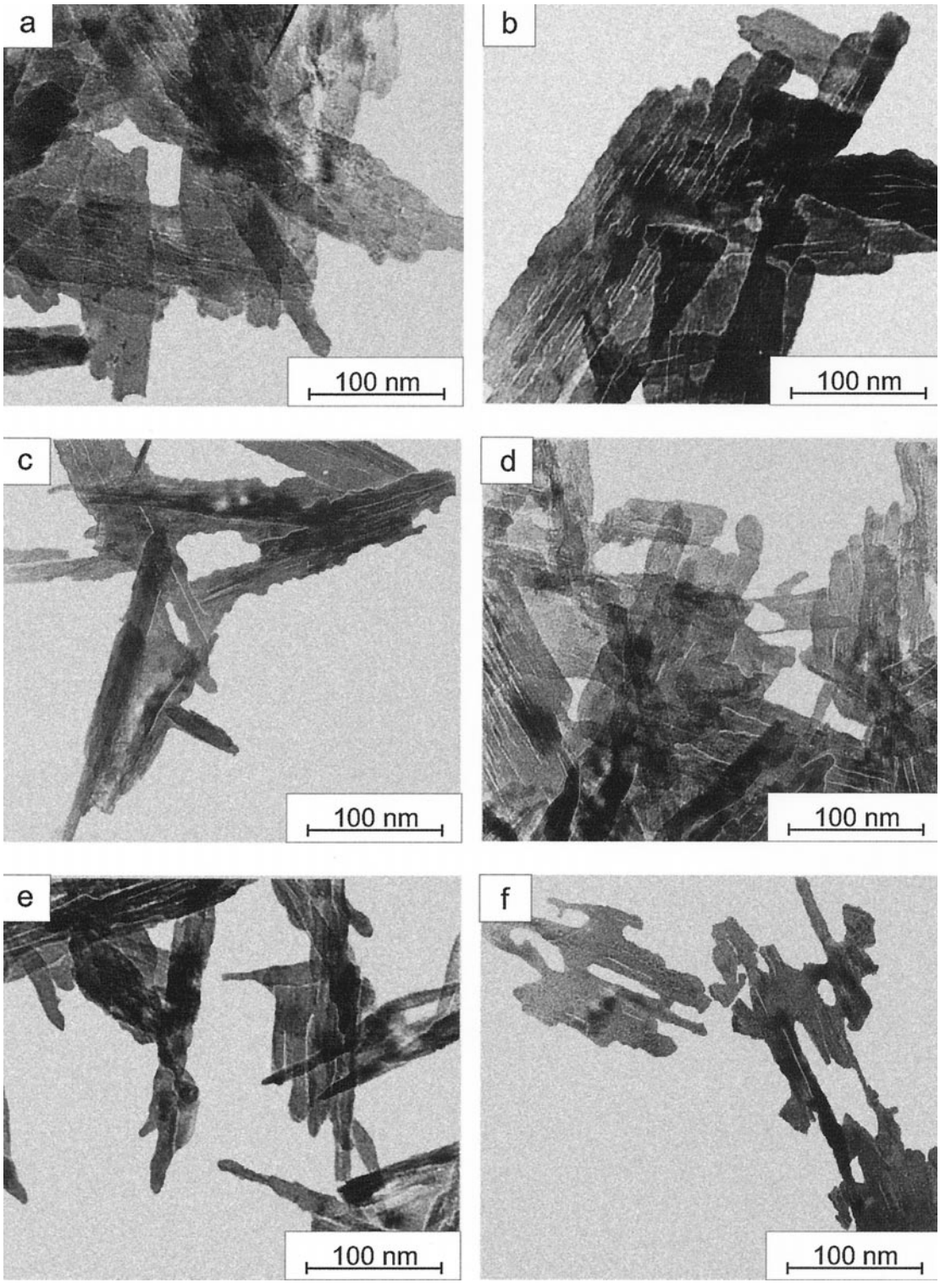

Fig. 4. Transmission electron micrographs of the lepidocrocite L-5 as a function of dissolution: (a) $m/m_0 = 1$; (b) $m/m_0 = 0.8$; (c) $m/m_0 = 0.6$; (d) $m/m_0 = 0.4$; (e) $m/m_0 = 0.2$; (f) $m/m_0 = 0.05$).

lepidocrocite L-5 were taken from the reactor in the course of the reduction experiment and then examined with TEM. Selected micrographs taken at different stages of dissolution (m/m_0) are shown in Figure 4. Initially, ascorbic acid attacks the lepidocrocite crystals mainly on the basal surfaces, producing a slightly curved relief (Fig. 4a). From the ends of the crystals, preferential dissolution occurs at the crystallite boundaries along the c-axis (Fig. 4b). The crystallite boundaries

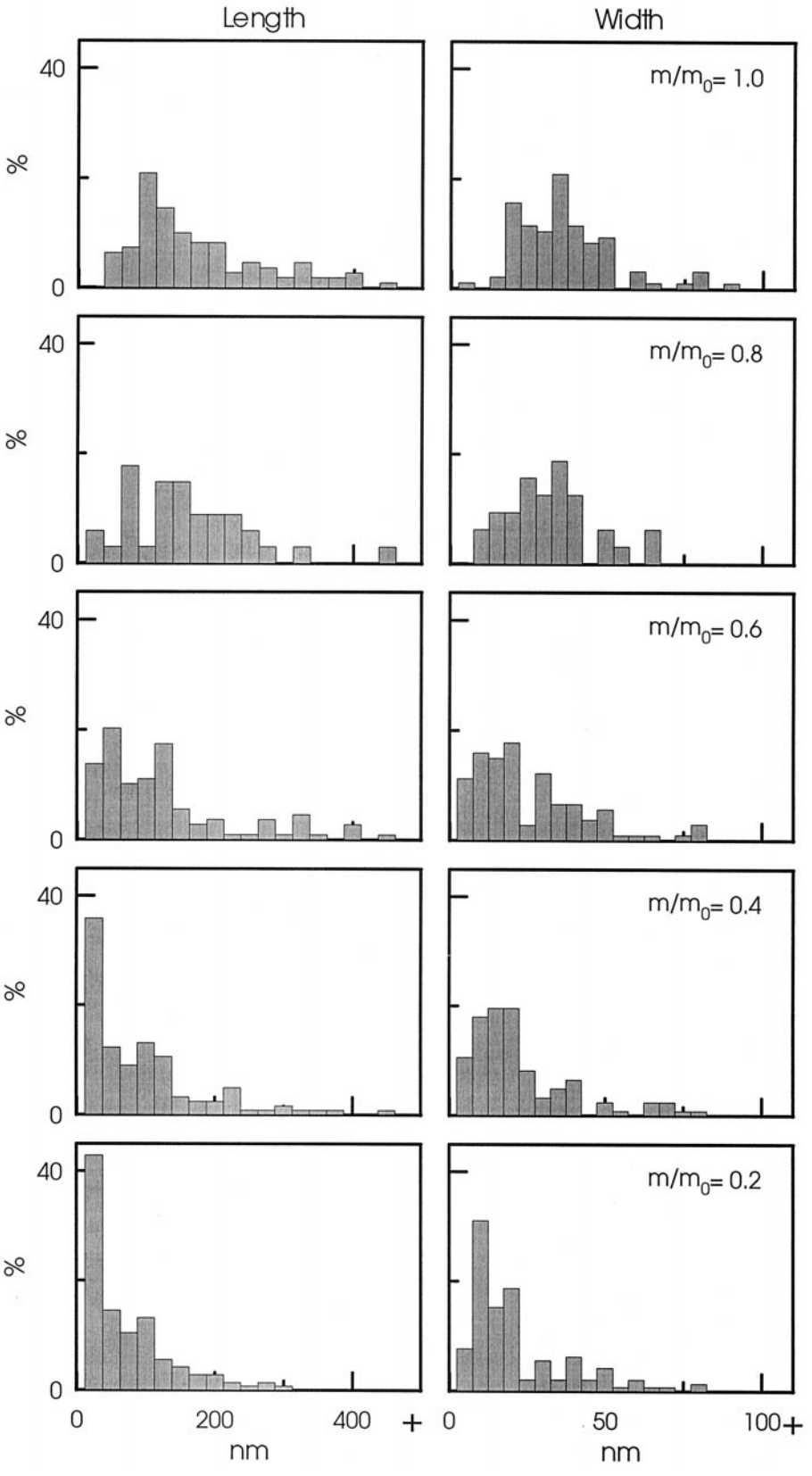

Fig. 5. Length and width distributions of lepidocrocite crystals of sample L-5, measured with TEM during dissolution.

develop into elongated cavities and, as a result, the ends of the crystals become highly irregular (Fig. 4c). It also appears that the crystals fall apart along these cavities parallel to the c-axis. In any case, the crystals in Figure 4c have a more slender appearance than in Figure 4b. During further dissolution, the elongated cavities get very pronounced and most corners are completely dissolved. Some crystals now have big cavities and many crystals are lengthwise separated (Fig. 4d). The last 20% of the crystals contain a large quantity of long, thin bars with highly curved surfaces (Fig. 4e). The crystals making up the last 5% of the sample are merely honeycomb remnants of the original crystals (Fig. 4f).

The length and width of 100 to 300 crystals were measured on TEM pictures at the different stages of dissolution. The results were divided into 18 size groups and are shown in Figure 5. Initially ($m/m_0 = 1$) the length of the crystals varies between 50 and 450 nm and the width between 15 and 80 nm. The size distribution is both for length and width slightly skewed towards smaller particles as compared to a normal distribution. When m/m_0 decreases from 1.0 to 0.8, the distribution of length and width changes towards shorter crystals. Going from $m/m_0 = 0.8$ *to* 0.6, there is a change in both the length and width distributions towards lower values. This change is probably associated with the crystals falling apart along the c-axis. Further dissolution is dominated by the development still smaller elongated crystals.

4. DISCUSSION

4.1. Rate Laws and Data Analysis

When $g(C)$ is kept constant in the course of the experiment then the general rate law of Christoffersen and Christoffersen (1976), Eqn. 1 reduces to (Postma, 1993):

$$\frac{J}{m_0} = k'\left(\frac{m}{m_0}\right)^{\gamma} \tag{2}$$

where k' is the product of the initial rate constant and $g(C)$. At initial conditions, $m/m_0 = 1$, the rate normalized to the initial mass equals the rate constant (k'). Eqn. 2 can be rewritten as:

$$\frac{J}{m_0} = \frac{\dfrac{-dm}{dt}}{m_0} = \frac{-d\left(\dfrac{m}{m_0}\right)}{dt} = k'\left(\frac{m}{m_0}\right)^{\gamma} \tag{3}$$

This equation can be integrated to give:

$$for\ \gamma = 1: ln\frac{m}{m_0} = -k'\,t + C_1 \rightarrow \frac{m}{m_0} = e^{-k't+C_1} \tag{4}$$

$$for\ \gamma \neq 1: \frac{\left(\dfrac{m}{m_0}\right)^{-\gamma+1}}{1-y} = -k'\,t + C_2 \rightarrow$$

$$\frac{m}{m_0} = [(-k'\,t + C_2)(1-\gamma)]^{\frac{1}{1-\gamma}} \tag{5}$$

The constants C_1 and C_2 are determined by applying the initial condition $m_{(t=0)} = 1$, which gives $C_1 = 0$ and $C_2 = 1/(1-\gamma)$, and consequently:

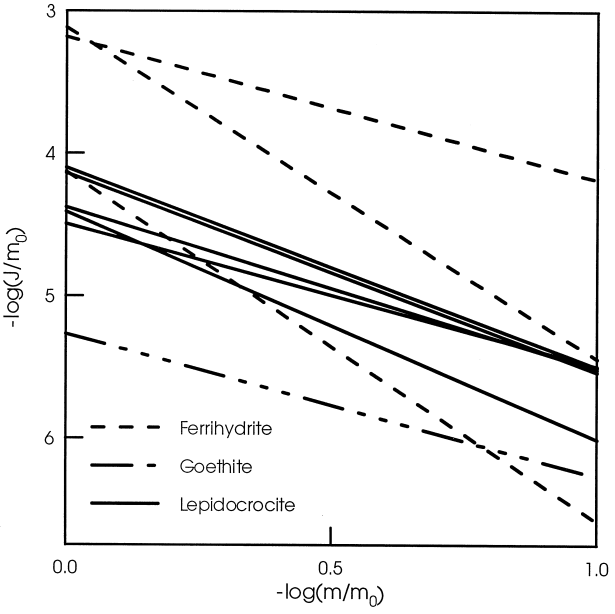

Fig. 6. Comparison of iron oxide reduction rates, normalized over initial mass (J/m_0) versus the fraction (m/m_0) remaining in the solid phase for lepidocrocite, ferrihydrite, and goethite.

$$for\ \gamma = 1: \frac{m}{m_0} = e^{-k't} \tag{6}$$

$$for\ \gamma \neq 1: \frac{m}{m_0} = [-k'(1-\gamma)t + 1]^{\frac{1}{1-\gamma}} \tag{7}$$

Equations 6 and 7 were fitted to the experimental data (m/m_0 vs. t) for the different iron oxides, using a nonlinear least squares procedure. The data fits are included as solid lines in Figures 2 and 3 and are seen to describe the experimental data well. In all cases the r^2 values of the data fits did exceed 0.98. The main discrepancy is found near the end of the experiments where experimental errors are largest. The values of k' and γ in Eqns. 6 and 7 as obtained for the different iron oxides are listed in Table 2. Also included in Table 2 is the initial surface flux, F, i.e., the rate constant k' normalized to surface area.

The rate equations of the different iron oxides are displayed in terms of $-\log(J/m_0)$ vs. $-\log(m/m_0)$ in Figure 6. For each iron oxide the rate equation is given as a straight line. At $-\log(m/m_0) = 0$, the value of $-\log(J/m_0)$ equals the rate constant, k', and the slope of the line corresponds to the exponent γ (Eqn. 2). In the following, the differences in k' and γ among the iron oxides will be discussed separately.

4.2. Initial Rates and Iron Oxide Reactivity

Figure 6 illustrates the large variation in the rate constants for the iron oxides, which amounts to two orders of magnitude. Clearly, the 2-line ferrihydrites have by far the highest rate constants which are one order of magnitude higher than for the better crystalline 6-line ferrihydrite. The rate constants of the lepidocrocites are all of the same order and vary by less than a factor of three. The lowest rate constant is clearly found for the poorly crystalline goethite.

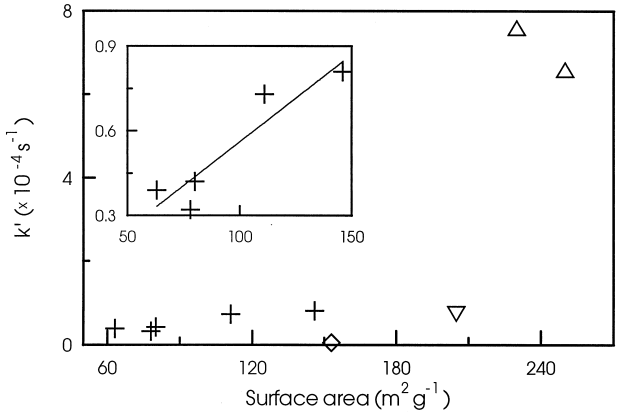

Fig. 7. The initial reduction rate as a function of specific surface area for lepidocrocite (+), 2Fer (Δ), 6Fer (▽), and goethite (◇).

The rate constants for the 2-line ferrihydrites are close to the results of Postma (1993) for reduction of ferrihydrite by 10 mM ascorbic acid. Zinder et al. (1986) found for a well crystalline goethite reacting with 1 mM ascorbate, conditions where the surface of goethite probably is saturated with ascorbate, an initial surface flux of 1.8×10^{-11} mol/m^2/s, which is considerable lower than found here (Table 2) for poorly crystalline goethite. Finally, Banwart et al. (1989) reported for hematite dissolution, at surface saturation with ascorbate, an initial surface flux of 6.1×10^{-11} mol/m^2/s. The general order of reactivity for different iron oxides reacting with ascorbic acid, corresponds well to the results of Canfield et al. (1992) and Dos Santos Afonso and Stumm (1992) obtained by reduction with H_2S.

Figure 7 displays a plot of the rate constants against the specific surface area of the different iron oxides. There is obviously no simple relationship between the surface area and the reduction rate among different minerals, which emphasizes the importance of the crystal structure. The ferrihydrites have by far the highest specific surface flux but the use of the BET method for measurement of their specific surface area may be questionable (Cornell and Schwertmann, 1996). However, if a surface area of 1000 m^2/g is assumed then the ferrihydrites would attain a surface flux as low as found for the lepidocrocites.

For the group of lepidocrocites there is a good correlation ($r^2 = 0.87$) between the surface area and the rate constant. Considering the variability in crystal morphology (Fig. 1), the dominant influence of the specific surface area on the rate constant is remarkable. Finally, the goethite has a much lower initial surface flux than the other minerals.

4.3. The Change in Dissolution Rate During Bulk Dissolution

The decrease in reaction rate during bulk dissolution is given by the slope, γ, of the lines in Figure 6. For the 2-line ferrihydrites the γ of two apparently identical preparations varies from 1.0 to 2.3. The first γ value corresponds to what was reported by Postma (1993). However, the latter value reflects a more than a hundred-fold decrease in reaction rate at 90% dissolution ($m/m_0 = 0.1$), where the rate becomes comparable to that of lepidocrocite. A similar strong decrease in reaction rate is found for the 6-line ferrihydrite. According to Drits et al. (1993), ferrihydrite is composed of three distinct phases, ranging from a defective ferrihydrite structure to nano-crystalline hematite. The initial surface flux of well crystalline hematite was by Banwart et al. (1989) determined to be 6.1×10^{-11} mol/m^2/s which is about the same as the terminal dissolution rate for ferrihydrites with a high γ. Perhaps the proportion of nano-crystalline hematite in ferrihydrite determines the terminal dissolution rate.

For lepidocrocite, the values of γ varied in the range of 1.0 to 1.6. TEM photographs showed the samples L-1 to L-3 to consist of predominantly single domain crystals, which yielded γ-values of 1.4-1.6. Samples L-4 and L-5 are in contrast mainly multidomainic and result in γ values of 1.0 and 1.1. These significant lower γ values probably reflects the tendency of multidomainic crystals to disintegrate during dissolution, as was documented for sample L-5 (Fig. 4). Finally for goethite a γ value of 1.0 is found. For comparison, Cornell et al. (1974, 1975, 1976) studied complete dissolution of goethites with different crystal morphologies in 0.5 M HCl. A fit of Eqn. 2 to this data yielded γ-values ranging from 0.68 to 1.0.

The parameter γ collects in reality the effects of a variety of processes. First of all, during dissolution the ratio between surface area and mass must change. Secondly, the grain size distribution is of importance as the finest particles are selectively dissolved. Thirdly, the reactive site density may change during dissolution. Finally, as has been demonstrated for one of the lepidocrocites, disintegration of crystals may also be of importance.

As discussed previously, the relation between surface area and mass predicts for isometric bodies, such as cubes or spheres, a γ of 2/3. The other geometric endmember would be a cylinder where the surface area of the terminal faces is negligible, perhaps as a analogue for the elongated shape of lepidocrocite crystals. For such a cylinder, γ would become 1/2. Thus, the relation between surface area and mass predicts that during dissolution the rate should change as a function of m/m_0, with γ-values in the range 1/2 to 2/3. The experimental data in Table 2 shows much higher γ-values, indicating the importance of additional factors.

The simple rate dependency on the change in surface area as a function of decreasing mass is in principle only valid for monodisperse crystal populations. As already demonstrated for lepidocrocite (Fig. 5) the variation in crystal size in our mineral preparations is large. Generally, a wider grain size distribution is expected to yield a higher γ-value. Taplin (1974) and Dixon and Hendrix (1993) analyzed the effect of various lognormal grainsize distributions on the γ-value and found that values up to 3.4 are possible. In order to further quantify the effect of the grain size distribution on the resulting γ-value, values of m/m_0 vs. time were calculated for some typical particle size distributions shown in Figure 8a. The initial grain size distributions are considered to consist of spherical particles that dissolve at a constant rate per surface area. The mass of each size class of spheres was calculated for every time step and Eqn. 7 was then fitted to the simulated m/m_0 and time data. The results (Fig. 8b) show that both a bimodal and a strongly skewed grain size

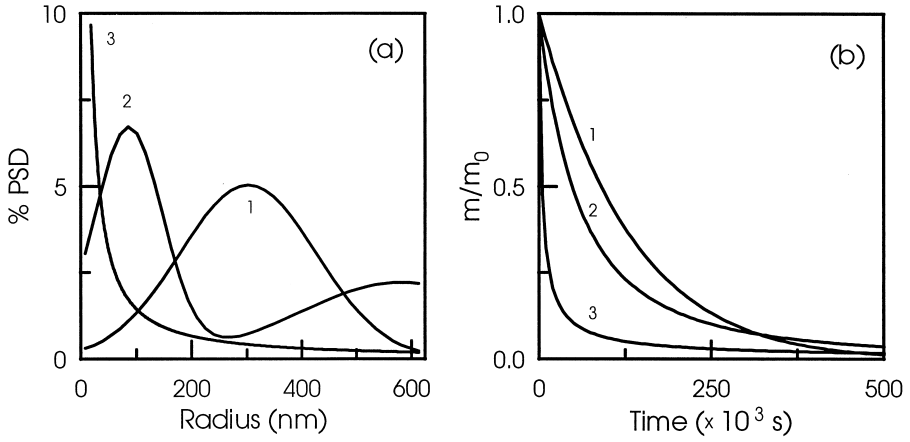

Fig. 8. Results of simulated dissolution experiments. (a) Different particle size distributions (PSD, in percentage) represented by 1: normal distribution, 2: bimodal distribution, and 3: lognormal distribution. (b) Bulk dissolution kinetics; m/m_0 is the undissolved mineral fraction. The γ-value for the different distributions are 1 : 0.9; 2 : 1.5, and 3 : 2.2.

distribution may yield a γ-value significantly higher than 2/3. Clearly, the grain size distribution has a major impact on the resulting value of γ.

The individual iron oxide particles are composed of domains, or crystallites, held together by bonds weaker than the interatomic bonds within the crystallites. The crystallite size distribution of the lepidocrocites was calculated by applying the Warren–Averbach theory to XRD line broadening. The mean crystallite size, derived from XRD did correlate with the surface area of the different mineral preparations (data not shown). The TEM observations of L-5 showed the crystals to break apart along domain boundaries during dissolution, indicating that these subunits, at some point during reaction, determine the surface area. In this sense, the crystallite size distribution can be used as a proxy of the effective particle size distribution.

The crystallite size distribution derived from XRD for the lepidocrocites and the initial particle size distribution observed in TEM for L-5 (Fig. 5) were used for a numerical simulation of the dissolution kinetics. The crystallites were simulated to dissolve as spheres with a constant surface flux (6×10^{-9} mol/m^2/s). Equations 6–7 were fitted to the simulated m/m_0 vs. time data and the resulting γ and k values are shown in Figure 9, plotted vs. the experimentally determined values.

The rate constants predicted from the crystallite size distributions clearly correlate with the experimental rate constants and the ratio between the two is close to unity. This illustrates that surface area and crystallite size are related parameters. Mineral dissolution is on an atomic scale often controlled by the density of dislocations and other high-energy sites. Our data suggest that for lepidocrocite the bulk parameters surface area and particle size distribution may describe the observed variation in initial dissolution rate. For lepidocrocite, the initial number of high-energy surface sites must therefore be a linear function of the surface area. The γ-values predicted from crystallite and particle size distribution were lower than the experimental values. The observed decrease in dissolution rate during the experiment is thus higher than predicted from the particle size distribution combined with a constant surface flux.

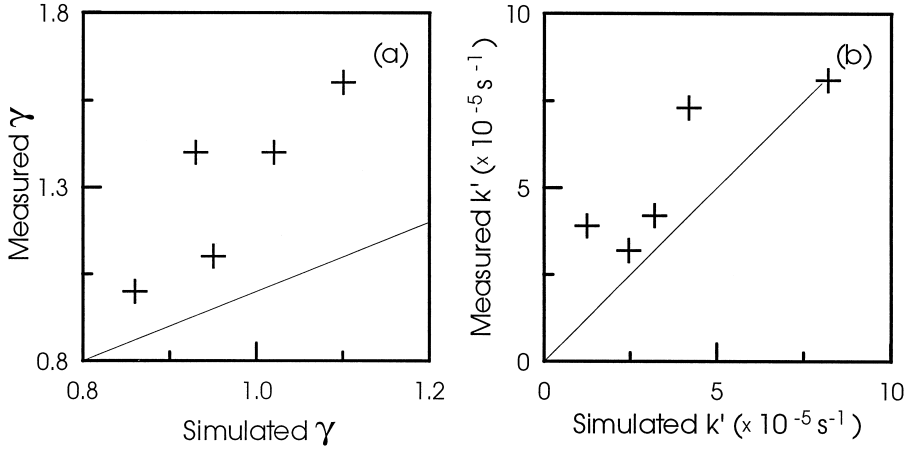

Fig. 9. Plot of the experimentally obtained γ (a) and k′ (b) values and γ and k' values predicted by particle size distributions from XRD. Lines represent a 1 : 1 relationship.

It suggests that there is change in mechanism during dissolution which is in accord with the microscopic evidence.

4.4 Implications for Natural Environments

In a general sense, the results displayed in Figure 6 demonstrate that the change in reduction rate during bulk dissolution of iron oxides is on the same order of magnitude as the variation in initial rates among different iron oxides and is therefore an important parameter. In natural sediments, the change in iron oxide reactivity during dissolution is even larger (Postma, 1993; Larsen, 1998). Also, the variation in rate due to variable reactivity may exceed the effect of different reductants (Postma, 1993). Given the heterogeneity of the pool of iron oxides in sediments, it may be anticipated that the kinetics of iron oxide reduction must play an important role for the rate of organic matter degradation in sediments. The exact role will depend on the balance between the rate of organic matter degradation and the rate of iron reduction (Postma and Jakobsen, 1996). In an overall sense, the two processes proceeds sequentially with organic matter fermentation producing intermediates like H_2 and acetate, which are subsequently consumed by iron(III) reduction. If abundant reactive organic material is available the rate of organic matter fermentation is likely to exceed the rate of iron oxide reduction and the kinetics of iron oxide reduction will be rate limiting. Simultaneous processes, such as sulfate reduction or methanogenesis, are likely to proceed. If, on the other hand, abundant reactive iron is available but little reactive organic matter, then the kinetics of organic matter fermentation becomes overall rate determining, whereas sulfate reduction and methanogenesis will not occur.

Accordingly, it is the balance of the kinetics of organic matter degradation versus the kinetics of iron oxide reduction that to a large extent determines the energy flow during organic matter degradation in anoxic sediments.

5. CONCLUSIONS

The reactivity of iron oxides during complete reductive dissolution in 10 mM ascorbic acid may be described using the equation:

$$\frac{J}{m_0} = k'\left(\frac{m}{m_0}\right)^{\gamma} \tag{8}$$

Initial rates, k', varied by two orders of magnitude among the iron oxides, ranging from about $7 \times 10^{-4} \cdot s^{-1}$ for 2-line ferrihydrite over $5 \times 10^{-5} \cdot s^{-1}$ as a typical value for lepidocrocite to $5.4 \times 10^{-6} \cdot s^{-1}$ for a poorly crystalline goethite. Among different iron oxides, the initial rates were independent of the specific surface area, emphasizing the importance of mineralogy. However, among the group of five lepidocrocites the initial rate was proportional to the specific surface area.

The change in rate during complete dissolution of a crystal population was evaluated by using in an exponential function of the remaining mass of mineral. The exponent γ was found to vary from 1.0 to 2.3 for ferrihydrites, whereas for lepidocrocite the range was 1.0–1.6 and for goethite 1.0.

Different factors influence the γ value; the relation between mass and surface area of crystals, the crystal size distribution, the reactive site density, and finally as shown for lepidocrocite, the crystals falling apart due to preferential dissolution along crystallite boundaries. Of these factors, the particle size distribution appear to be one of the most important for the reductive dissolution of lepidocrocite.

Acknowledgments—This research was supported by the Groundwater Research Centre through grants from the Danish Technical Research Council. We thank Niels Peter Arildskov, Liselotte Clausen, Rasmus Jakobsen, Joan Jensen, Christian Koch, Flemming Kragh, Thomas Richter, Stephen Talman, and Ellen Zimmer for fruitful discussions and assistance with experimental work. Careful reviews from Dr. G. Sposito and two anonymous reviewers were much appreciated.

Associate editor: G. Sposito

REFERENCES

Albrechtsen H.-J. and Christensen T. (1994) Evidence for microbial iron reduction in a landfill leachate-polluted aquifer (Vejen, Denmark). *Appl. Environ. Microbiol.* **60,** 3920–3925.

Banwart S., Davies S., and Stumm W. (1989) The role of oxalate in accelerating the reductive dissolution of hematite (α-Fe_2O_3) by ascorbate. *Colloids Surfaces* **39,** 303–309.

Biber M. V., Dos Santos Afonso M., and Stumm W. (1994) The coordination chemistry of weathering: IV. Inhibition of the dissolution of oxide minerals. *Geochim. Cosmochim. Acta* **83,** 1999–2010.

Canfield D. E. (1989) Reactive iron in marine sediments. *Geochim. Cosmochim. Acta* **53,** 619–632.

Canfield D. E., Raiswell R., and Bottrell S. (1992) The reactivity of sedimentary iron minerals toward sulfide. *Am. J. Sci.* **292,** 659–683.

Canfield D. E., Thamdrup B., and Hansen J. W. (1993) The anaerobic degradation of organic matter in Danish coastal sediments: Iron reduction, manganese reduction, and sulfate reduction. *Geochim. Cosmochim. Acta* **57,** 3867–3883.

Christoffersen J. and Christoffersen M. R. (1976) The kinetics of dissolution of calcium sulphate dihydrate in water. *J. Crystal Growth* **35,** 79–88.

Christoffersen J., Christoffersen M. R., and Kjaergaard N. (1978) The kinetics of dissolution of calcium hydroxyapatite in water at constant pH. *J. Crystal Growth* **43,** 501–511.

Cornell R. M., Posner A. M., and Quirk J. P. (1974) Crystal morphology and the dissolution of goethite. *J. Inorg. Nucl. Chem.* **36,** 1937–1946.

Cornell R. M., Posner A. M., and Quirk J. P. (1975) The complete dissolution of goethite. *J. Appl. Chem. Biotechnol.* **25,** 701–706.

Cornell R. M., Posner A. M., and Quirk J. P. (1976) Kinetics and mechanisms of the acid dissolution of goethite (α-FeOOH). *J. Inorg. Nucl. Chem.* **38,** 563–567.

Cornell R. M. and Schwertmann U. (1996) *The Iron Oxides.* VCH Verlagsgesellschaft.

Deng Y. and Stumm W. (1994) Reactivity of aquatic iron(III) oxyhydroxides-implications for redox cycling of iron in natural waters. *Applied Geochem.* **9,** 23–36.

Dixon D. G. and Hendrix J. L. (1993) Theoretical basis for variable order assumption in the kinetics of leaching of discrete grains. *AIChE J.* **39,** 904–907.

Dos Santos Afonso M. and Stumm W. (1992) Reductive dissolution of iron(III) (hydr)oxides by hydrogen sulfide. *Langm.* **8,** 1671–1675.

Dos Santos Afonso M., Morando P. J., Blesa M. A., Banwart S., and Stumm W. (1990) The reductive dissolution of iron oxides by ascorbate. *J. Colloid Interface Sci.* **138,** 74–82.

Drits V. A., Sakharov B. A., Salyn A. L., and Manceau A. (1993) Structural model for ferri hydrite. *Clay Minerals* **28,** 185–207.

Heron G., Crouzet C., Bourg A. C. M., and Christensen T. H. (1994) Speciation of Fe(II) and Fe(III) in contaminated aquifer sediments using chemical extraction techniques. *Environ. Sci. Technol.* **28,** 1698–1705.

Jakobsen R. and Postma D. (1999) Redox zoning, rates of sulfate reduction and interactions with Fe-reduction and methanogenesis in a shallow sandy aquifer, Rømø, Denmark *Geochim. Cosmochim. Acta* **63,** 137–151.

Larsen O. (1998) Reactivity of Iron(III) oxides and Iron(III) oxide reduction in a shallow aquifer. Ph.D. thesis, Technical Univ. Denmark.

Lovley D. R. (1991) Dissimilatory Fe(III) and Mn(IV) reduction. *Microbiol. Rev.* **55,** 259–287.

Lyngkilde J. and Christensen T. H. (1992) Redoxzones of a landfill leachate pollution plume Vejen Denmark. *J. Contam. Hydrol.* **10,** 273–289.

Mehra O. P. and Jackson M. L. (1960) Iron oxide removal from soils and clays by a dithionite-citrate system buffered with sodium bicarbonate. *Clays Clay Mineral* **7,** 317–327.

Munch J. C. and Ottow J. C. G. (1980) Preferential reduction of amorphous to crystalline iron oxides by bacterial activity. *Soil Sci.* **129,** 15–21.

Nowack B. and Sigg L. (1997) Dissolution of Fe(III)(hydr)oxides by metal-EDTA complexes. *Geochim. Cosmochim. Acta* **61,** 951–963.

Postma D. (1993) The reactivity of iron oxides in sediments: a kinetic approach. *Geochim. Cosmochim. Acta* **57,** 5027–5034.

Postma D. and Jakobsen R. (1996) Redox zonation: equilibrium constraints on the Fe(III)/SO_4-reduction interface. *Geochim. Cosmochim. Acta* **60,** 3169–3175.

Pulgarin C. and Kiwi J. (1995) Iron oxide-mediated degradation, photodegradation, and biodegradation of aminophenols. *Langm.* **11,** 519–526.

Raiswell R. and Canfield D. E. (1998) Sources of iron for pyrite formation in marine sediments. *Am. J. Sci.* **298,** 219–245.

Roden E. E. and Zachara J. M. (1996) Microbial reduction of crystalline iron(III) oxides: Influence of oxide surface are and potential for cell growth. *Env. Sci. Techn.* **30,** 1618–1628.

Roden E. E. and Urrutia M. M. (1999) Ferrous iron removal promotes microbial reduction of crystalline iron (III) oxides. *Env. Sci. Techn.* **33,** 1847–1853.

Schwertmann U. and Cornell R. M. (1991) *Iron Oxides in the Laboratory.* VCH verlagsgesell schaft.

Sidhu P. S., Gilkes R. J., Cornell R. M. Posner A. M., and Quirk J. P. (1981) Dissolution of iron oxides and oxyhydroxides in hydrochloric and perchloric acids. *Clays Clay Minerals* **29,** 269–276.

Stookey L. L. (1970) Ferrozine—a new spectrophometric reagent for iron. *Anal. Chem.* **42,** 779–781.

Sulzberger B., Suter D., Siffert C., Banwart S., and Stumm W. (1989) Dissolution of Fe(III)(hydr)oxides in natural waters: Laboratory assessment on the kinetics controlled by surface coordination. *Mar. Chem.* **28,** 127–144.

Suter D., Banwart S., and Stumm W. (1991) Dissolution of hydrous iron(III) oxides by reductive mechanisms. *Langm.* **7,** 809–813.

Taplin J. H. (1974) Index of reaction—a unifying concept for the reaction kinetics of powders. *J. Am. Ceram. Soc.* **57,** 140.

Thamdrup B., Finster K., Hansen J. W., and Bak F. (1993) Bacterial disproportionation of elemental sulfur coupled to chemical reduction of iron and manganese. *Appl. Environ. Microbiol.* **59,** 101–108.

van Breemen N. (1988) Effects of seasonal redox processes involving iron on the chemistry of periodically reduced soils. In *Iron in Soils and Clay Minerals* (eds. J. W. Stucki, B. A. Goodmann, and U. Schwertmann), Chap. 23, pp. 797–809. D. Reidel.

Win-Crysize (1996). Win-Crysize ver. 3.0. Crystallite Size and Strain. *Siemens.*

Yao W. and Millero F. J. (1996) Oxidation of hydrogen sulfide by hydrous Fe(III) oxides in seawater. *Mar. Chem.* **52,** 1–16.

Zinder B., Furrer G., and Stumm W. (1986) The coordination chemistry of weathering: II Dissolution of Fe(III) oxides. *Geochim. Cosmochim. Acta* **50,** 1861–1869.